Journal of Power Sources 273 (2015) 554–560

Contents lists available at ScienceDirect

Journal of Power Sources

journal homepage: www.elsevier.com/locate/jpowsour

High-performance nickel–platinum nanocatalyst supported on mesoporous alumina for hydrogen generation from hydrous hydrazine

Yuanyuan Jiang [a], Qiang Kang [b], Jingjing Zhang [a], Hong-Bin Dai [a, *], Ping Wang [a, *]

[a] Shenyang National Laboratory for Materials Science, Institute of Metal Research, Chinese Academy of Sciences, 72 Wenhua Road, Shenyang 110016, PR China

[b] Analysis & Testing Division, Institute of Metal Research, Chinese Academy of Sciences, 72 Wenhua Road, Shenyang 110016, PR China

HIGHLIGHTS

- A newly synthesized Ni–Pt/meso-Al_2O_3 catalyst is reported.
- The catalyst shows excellent activity for selective decomposition of $N_2H_4 \cdot H_2O$ to H_2.
- The Ni-based catalyst may promote the application of $N_2H_4 \cdot H_2O$ as a viable H_2 carrier.

GRAPHICAL ABSTRACT

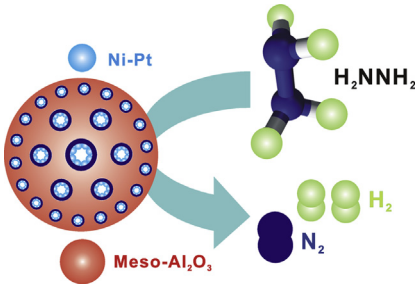

ARTICLE INFO

Article history:
Received 21 July 2014
Received in revised form
18 September 2014
Accepted 18 September 2014
Available online 28 September 2014

Keywords:
Decomposition
Hydrogen generation
Hydrous hydrazine
Mesoporous alumina
Nickel–platinum alloy nanocatalyst

ABSTRACT

The catalyst with high activity, 100% selectivity and good durability is highly desirable in developing a hydrous hydrazine-based hydrogen generation system. Herein we report the synthesis of nickel–platinum (Ni–Pt) bimetallic nanoparticles supported on mesoporous alumina (MA) using a simple one-pot evaporation-induced self-assembly method. The Ni–Pt/MA catalyst exhibits excellent activity and satisfactory stability for selectively catalyzing the decomposition of hydrous hydrazine to generate hydrogen at mild temperatures, which compares favorably with the performance of the catalysts developed to date. The facile synthesis of high-performance and cost-effective Ni-based catalyst is of clear significance for the development of hydrous hydrazine as a viable hydrogen carrier.

1. Introduction

Hydrogen storage is a key enabling technology for the extensive use of H_2 as an energy carrier. For a long period, the materials capable of reversible dehydrogenation were prized in hydrogen storage research. But decades of intensive studies on metal hydrides, complex hydrides and physisorbents led to no viable material that can reversibly store large amount of H_2 at moderate temperatures with fast kinetics [1,2]. This situation stimulated the development of chemical hydrogen storage technology as an alternative solution for mobile and portable H_2 source applications [3–5]. Among the materials of interest, hydrazine monohydrate ($N_2H_4 \cdot H_2O$) is a less well explored but very promising candidate [6,7]. $N_2H_4 \cdot H_2O$ is a liquid-phase material that can be safely stored under ambient conditions. This offers a clear potential to take advantage of the existing liquid-based distribution infrastructure. $N_2H_4 \cdot H_2O$ has a high hydrogen density (8 wt%), a relatively low cost and is readily available. Importantly, the decomposition of

* Corresponding authors. Tel.: +86 24 2397 1622; fax: +86 24 2389 1320.
E-mail addresses: hbdai@imr.ac.cn (H.-B. Dai), pingwang@imr.ac.cn (P. Wang).

http://dx.doi.org/10.1016/j.jpowsour.2014.09.119
0378-7753/

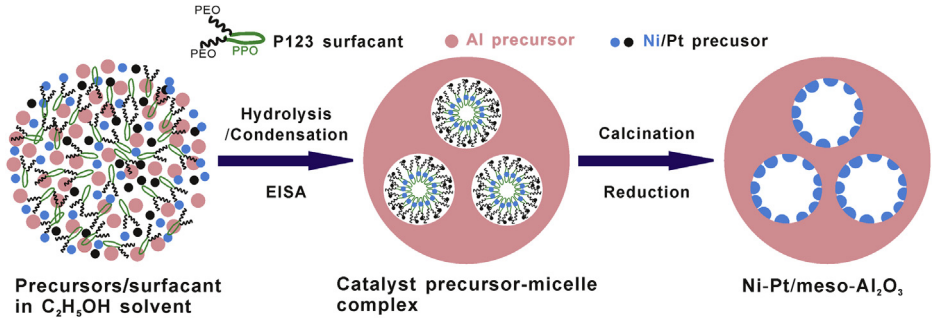

Fig. 1. Schematic diagram of the preparation of Ni–Pt bimetallic catalyst supported on mesoporous alumina.

$N_2H_4{\cdot}H_2O$ does not generate any solid byproducts, which is of great benefit for the design of hydrogen source system. The combination of these favorable attributes makes $N_2H_4{\cdot}H_2O$ an even more competitive hydrogen carrier compared with the previously extensively studied chemical hydrides, like sodium borohydride ($NaBH_4$) and ammonia borane (NH_3BH_3).

$$N_2H_4 \rightarrow N_2 + 2H_2, \quad \Delta H = -95.4 \text{ kJ mol}^{-1} \tag{1}$$

$$3N_2H_4 \rightarrow N_2 + 4NH_3, \quad \Delta H = -157 \text{ kJ mol}^{-1} \tag{2}$$

Hydrazine (N_2H_4) is the effective hydrogen storage component of $N_2H_4{\cdot}H_2O$, which decomposes via two competitive reactions following Eqs. (1) and (2), respectively. From a perspective of hydrogen storage, Reaction (1) must be selectively promoted and Reaction (2) restrained. To this end, a number of transition metal catalysts or their alloys have been recently developed, like Ir/γ-Al_2O_3 [8], Ni–Al_2O_3–HT [9], FeB/MWCNTS [10], Ir, Rh [11], and Ni–M (M = Ir, Pt, Rh, Pd, Fe, Mo) [12–25]. These catalysts showed varied H_2 selectivity and catalytic activity towards the decomposition reactions of $N_2H_4{\cdot}H_2O$, from which two empirical rules can be derived. One is that alloying may remarkably enhance the catalytic activity and H_2 selectivity of the catalyst [12–18]. The other is that use of basic support to immobilize catalyst nanoparticles may render not only improved durability, but also enhanced H_2 selectivity [9,19–21,24,25]. In the past years, employment of alloying and/or immobilization strategies had yielded several novel catalysts, which enable selective decomposition of $N_2H_4{\cdot}H_2O$ to generate H_2 at mild conditions. But from a practical point of view, the currently available catalysts show only moderate catalytic activity and problematic durability, which causes problems on reaction kinetics and controllability of H_2 generation process. This necessitates further exploration of advanced catalyst for developing $N_2H_4{\cdot}H_2O$ as a viable hydrogen carrier.

Herein, we report the synthesis of Ni–Pt nanocatalyst supported on mesoporous alumina (denoted as Ni–Pt/MA) using a simple one-pot method. The Ni–Pt/MA catalyst shows excellent activity and satisfactory stability for selectively catalyzing the decomposition of $N_2H_4{\cdot}H_2O$ to generate H_2, which compares favorably with the catalysts developed to date.

2. Experimental

2.1. Chemicals and preparation of the catalysts

Nickel (II) acetylacetonate ($Ni(acac)_2$, 95%), chloroplatinic acid ($H_2PtCl_6{\cdot}6H_2O$, Pt content $\geq$ 37%), aluminum isopropoxide ($Al(OC_3H_7)_3$, 99.99%), anhydrous ethanol (C_2H_5OH, 99%) and nitric acid (HNO_3, 67%) were purchased from Aladdin. $(EO)_{20}(PO)_{70}(EO)_{20}$ triblock copolymer (Pluronic P123, typical Mn = 5800) was purchased from Sigma–Aldrich and $N_2H_4{\cdot}H_2O$ (99%) from Alfa Aesar. All chemicals were used as received.

The catalysts with varied alloy compositions but fixed alloy/support molar ratio, 20 mol% (Ni_{100-x}–Pt_x)/80 mol% MA (x = 0, 3, 5, 7, 10, 13, 15 and 100, respectively), were prepared using a one-pot evaporation-induced self-assembly (EISA) method [26–28]. In a typical synthesis procedure, 1.60 g of Pluronic P123 surfactant, 2.0 mmol of $Ni(acac)_2$ and H_2PtCl_6 with an expected stoichiometric ratio were dissolved in 12 mL of C_2H_5OH (denoted as solution A) at 40 °C, then another solution B containing 20 mL of C_2H_5OH, 3.27 g of $Al(OC_3H_7)_3$ (16 mmol, corresponding to 8 mmol of Al_2O_3) and 2.6 mL of HNO_3 was added into solution A under magnetic stirring. The solution mixture was sealed and continuously stirred for 5 h, and then transferred to an oven at 60 °C for evaporation of C_2H_5OH for 48 h. The as-prepared xerogel was calcined at 400 °C in air for 4 h to remove the template, followed by reduction under H_2 atmosphere for another 1.5 h. All the as-prepared catalysts were stored in an Ar-filled glove box to avoid oxidation.

2.2. Catalyst performance testing

The catalytic decomposition of $N_2H_4{\cdot}H_2O$ was conducted in a 50 mL two-neck flask under magnetic stirring. During the measurement, the flask was placed in a thermostat that was equipped with a water circulating system to maintain the reaction temperature, typically within ±0.5 °C. In a typical measurement run, the alkaline $N_2H_4{\cdot}H_2O$ solution was pre-heated and held at the

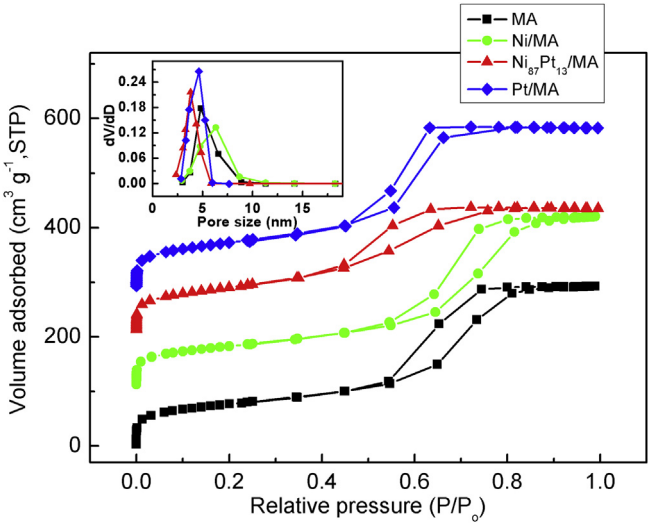

Fig. 2. Adsorption/desorption isotherms and pore size distributions (inset) of the pristine MA and MA-supported catalyst.

Table 1
Adsorption parameters, metal grain size, particle size and lattice constant of various samples.

Samples	Adsorption parameters			Metal grain size (nm)[d]	Metal particle size (nm)[e]	Lattice constant (Å)[f]
	BET ($m^2\ g^{-1}$)[a]	V_p ($cm^3\ g^{-1}$)[b]	D_p (nm)[c]			
MA	274	0.46	5.3	–	–	–
Ni/MA	260	0.49	5.8	3.4	3.8	3.52
$Ni_{97}Pt_3$/MA	302	0.36	3.3	2.6	2.8	3.60
$Ni_{93}Pt_7$/MA	295	0.41	3.6	2.1	2.4	3.63
$Ni_{87}Pt_{13}$/MA	290	0.37	3.8	1.8	1.9	3.65
Pt/MA	298	0.47	4.2	7.0	7.4	3.89

[a] BET specific surface area.
[b] Total pore volume was obtained at $P/P_0 = 0.99$.
[c] Average pore diameter was calculated by BJH method using the desorption isotherm branch.
[d] Metal grain size was estimated from the XRD result.
[e] Metal particle size was determined by the TEM morphology observation.
[f] The lattice constant value was determined from the XRD result.

designated temperature, and then the powdery catalyst attached on a magnetic stirring bar was dropped into the solution to initiate the decomposition reaction. The gaseous products were allowed to pass through a trap containing 1 M HCl to absorb NH_3, if any, and then measured by a gravimetric water-displacement method using an electronic balance with an accuracy of 0.01 g. The weight data were automatically recorded by data acquisition software (one datum every 10 s) and the determined gas amount was normalized to standard condition.

In determination of the reaction rate (h^{-1}), all the Ni and Pt atoms were assumed to take part in the catalytic reaction and the time required for a 50% conversion of $N_2H_4 \cdot H_2O$ was used in calculation [14,19]. The selectivity towards H_2 generation (X) was calculated following Eq. (3), which can be derived from Eqs. (1) and (2).

$$X = \frac{3Y-1}{8}\left[Y = \frac{n(N_2)+n(H_2)}{n(N_2H_4)}\right] \quad (3)$$

2.3. Characterization of the catalysts

The catalyst samples were characterized by powder X-ray diffraction (XRD, Rigaku D/MAX-2500, Cu Kα radiation), X-ray photoelectron spectroscopy (XPS, ESCALAB 250, Al Kα X-ray source) and transmission electron microscopy (TEM, FEI Tecnai F20), which is equipped with an energy dispersive X-ray spectroscopy (EDS) analysis unit. In the XPS measurements, high-resolution scans of elemental lines were recorded at 50 eV pass energy of the analyzer. All the binding energies (BEs) were calibrated using the C 1s peak (at 284.6 eV) of the adventitious carbon as an internal standard. The curve fitting was performed using XPS PEAK 4.1 software. In preparation of the TEM sample, the catalyst powder was first dispersed in

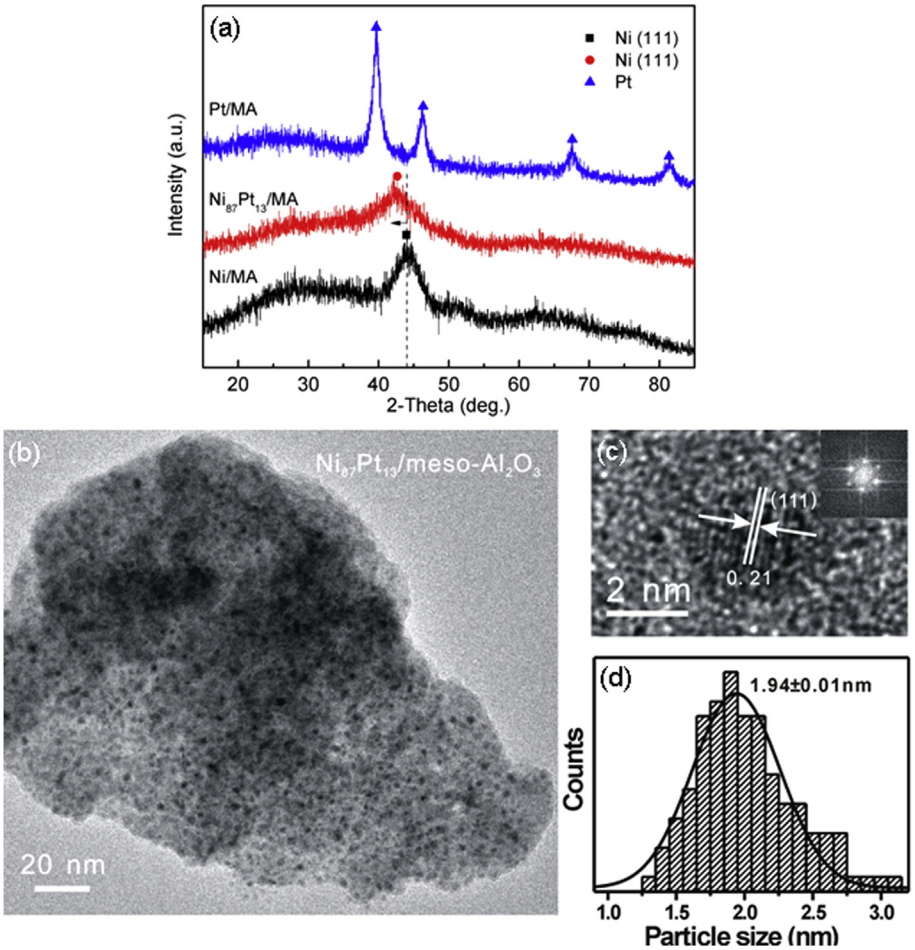

Fig. 3. (a) XRD patterns of Ni/MA, $Ni_{87}Pt_{13}$/MA and Pt/MA catalyst samples; (b) TEM image, (c) HRTEM image (inset: FFT spectrum) and (d) metal particle size distribution of $Ni_{87}Pt_{13}$/MA catalyst.

C_2H_5OH solution by ultrasound and then deposited on a copper grid coated with a holy carbon film. The specific surface area, total pore volume and average pore size of the catalyst sample were measured by N_2 adsorption/desorption isotherm at 77 K using the Brunauer–Emmett–Teller (BET) method and Barrett–Joyner–Halenda (BJH) model in a Micromeritics ASAP 2010 apparatus. Before each measurement, the sample was degassed in vacuum at 200 °C for 4 h. Element analyses of the catalyst samples were conducted in an inductively coupled plasma-atomic emission spectrometry (ICP-AES, Iris Intrepid).

3. Results and discussion

A series of MA-supported monometallic Ni, Pt and bimetallic Ni–Pt catalysts were synthesized using a one-pot EISA method, as schemed in Fig. 1. Evaporation induces micelle formation and concurrent partitioning of the Ni and/or Pt precursors into the micellar interiors and the alumina precursors surrounding the micellar exteriors [29,30]. After removing the template through calcination and following a reduction process, the alumina (Al_2O_3) forms a stable mesoporous skeleton and the metal nanoparticles are uniformly dispersed in the pore channels of the MA.

Fig. 2 presents the nitrogen adsorption/desorption isotherms and the pore size distributions of the pristine MA and various MA-supported catalysts. It was observed that all the samples showed type IV isotherms with H1 hysteresis loops, which were characteristic for mesoporous materials with "cylindrical-shaped" channels. But in the parallel low-angle XRD analysis, we did not observe diffraction peak at low angle range ($2\theta = 0.5–2°$). These results indicate that the MA prepared under the applied condition has long-range disordered mesoporous structure. Comparison of the adsorption parameters of the various samples (see in Table 1) found that metal-loading on MA to a molar ratio of 1:4 exerts no significant influence on specific surface area, pore volume and pore diameter. This indicates an important advantage of the one-pot EISA method over the traditional impregnation method, which often causes pore blockage or even damage of the support materials [27].

Fig. 3a shows the XRD patterns of Ni/MA, Pt/MA and Ni–Pt/MA catalysts. It was observed that the characteristic diffraction peaks of γ-Al_2O_3 were absent in all the catalyst samples, indicating the amorphous nature of the alumina support. The Pt/MA catalyst clearly showed the well-indexed peaks of fcc Pt (PDF 65-2868). But in the Ni–Pt/MA catalyst, the diffraction peaks of Pt were observed to disappear. This, together with the observed shift of (111) peak of Ni (PDF 65-0380) towards lower angle, clearly indicates the formation of Ni–Pt alloy. As a consequence of the substitution of larger Pt atoms for the smaller Ni atoms, the lattice constant of fcc Ni increases with increasing the amount of Pt (see in Table 1). Meanwhile, it was found that increasing the Pt amount resulted in decrease of the average grain size, as determined by the Scherrer equation. Presumably, the formation of Ni–Pt alloy perturbs the crystal growth of Ni nanocrystallites. As seen in Fig. 3b, microstructure study of a representative $Ni_{87}Pt_{13}$/MA catalyst by TEM clearly showed a uniform dispersion of Ni–Pt alloy nanoparticles on the amorphous alumina matrix, with a narrow size distribution ~2 nm in diameter. According to HRTEM observation and fast Fourier transform (FFT) analysis, most Ni–Pt nanoparticles have single-crystal structure with a lattice fringe of 0.21 nm, which is larger than that of the (111) plane of fcc Ni (0.203 nm), indicating the alloying of Ni with Pt. These results agree well with those obtained from XRD analysis.

The catalytic properties of the series of Ni–Pt/MA catalysts for the decomposition reactions of $N_2H_4 \cdot H_2O$ were examined and compared with the corresponding monometallic catalysts. As shown in Fig. 4, Pt/MA catalyst was totally inactive, and the Ni/MA catalyst exhibited poor catalytic activity and moderate H_2 selectivity in catalytic decomposition of $N_2H_4 \cdot H_2O$. But upon combining the two elements together, the resulting Ni–Pt/MA catalysts showed drastically enhanced catalytic performance. For example, incorporation of only 3 mol% Pt into Ni/MA catalyst resulted in a ~6-fold enhancement in catalytic activity and an increased H_2 selectivity from 70% to 92%. When the Pt/Ni molar ratio was increased to 13:87, which has an actual composition of 19.8 mol% $Ni_{87.3}Pt_{12.7}$/81.2 mol% MA according to the elemental analyses results, the catalyst exhibited an optimal catalytic performance. It enables a complete decomposition of $N_2H_4 \cdot H_2O$ to generate H_2 within 5 min at 50 °C in the presence of 0.5 M NaOH. The reaction rate per unit mole of active site of the $Ni_{87}Pt_{13}$/MA catalyst is ~160 h^{-1} at 50 °C, which stands out as the top level of the $N_2H_4 \cdot H_2O$ decomposition catalysts reported to date (see in Table 2). Notably, NaOH plays an important role in the catalytic decomposition of $N_2H_4 \cdot H_2O$. A set of control experiments found that addition of appropriate amount of NaOH exerts remarkable promoting effects on both reaction rate and H_2 selectivity (see in Fig. 5). Similar phenomenon was repeatedly observed in the $N_2H_4 \cdot H_2O$ systems using noble or non-noble metal catalysts [15,18,21,22,25]. Currently, the mechanism underlying the promoting effects of NaOH is still unclear. One possible explanation is that a highly basic environment will restrain the formation of basic NH_3 [18,22]. Alternatively, hydroxyl ions may participate in the surface reaction and alter the reaction pathway.

The catalytic decomposition behaviors of $N_2H_4 \cdot H_2O$ over the $Ni_{87}Pt_{13}$/MA catalyst were further examined at varied

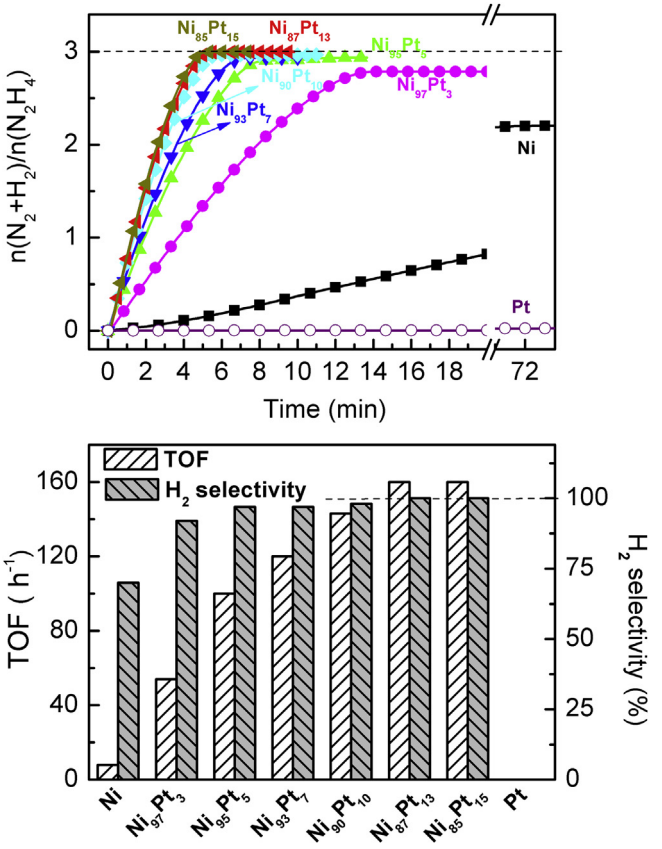

Fig. 4. Time course profiles (top) and Pt-content dependence of reaction rate and H_2 selectivity (bottom) of the system composed of 4 mL of 0.5 M $N_2H_4 \cdot H_2O$ + 0.5 M NaOH solution and Ni–Pt/MA catalysts at 50 °C. The catalyst/$N_2H_4 \cdot H_2O$ molar ratio was fixed at 1:10.

Table 2
A comparison of catalytic decomposition performance of $N_2H_4{\cdot}H_2O$ using $Ni_{87}Pt_{13}$/MA and other catalysts from open literature.

Catalyst	Reaction condition			TOF (h^{-1})	H_2 selectivity (%)	Ref.
	Catal./N_2H_4 (molar ratio)	NaOH (M)	T (°C)			
Ni/Al_2O_3	0.4	0	30	2.2	93	[9]
$Ni_{0.95}Ir_{0.05}$	0.1	0	25	1.6	100	[12]
$Ni_{0.99}Pt_{0.01}$	0.1	0	70	6	100	[13]
G4-OH ($Ni_{48}Pt_{12}$)	0.1	0.4	70	120	100	[15]
Rh_4Ni	0.1	0	25	3.8	100	[16]
$Ni_{50}Fe_{50}$	0.1	0.4	70	3.2	100	[18]
$Ni_{0.9}Pt_{0.1}/Ce_2O_3$	0.1	0.5	25	28.1	100	[21]
Rh_5Ni/GO	0.1	5	25	12	100	[22]
$Ni_{0.90}Pt_{0.05}Rh_{0.05}/La_2O_3$	0.1	0.5	25	45.9	100	[24]
$Ni_{64.1}Mo_{11.5}B_{24.4}/La(OH)_3$	0.3	2	50	13.3	100	[25]
$NiIr_{0.059}/Al_2O_3$	0.3	0	30	12.4	>99	[19]
			50	36.9	>99	
			70	84.3	97	
$NiPt_{0.057}/Al_2O_3$	0.3	0	30	16.5	97	[20]
			50	56.1	99	
			70	93.9	97	
$Ni_{87}Pt_{13}$/MA	0.1	0.5	30	50	100	This work
			50	160	100	
			70	492	100	

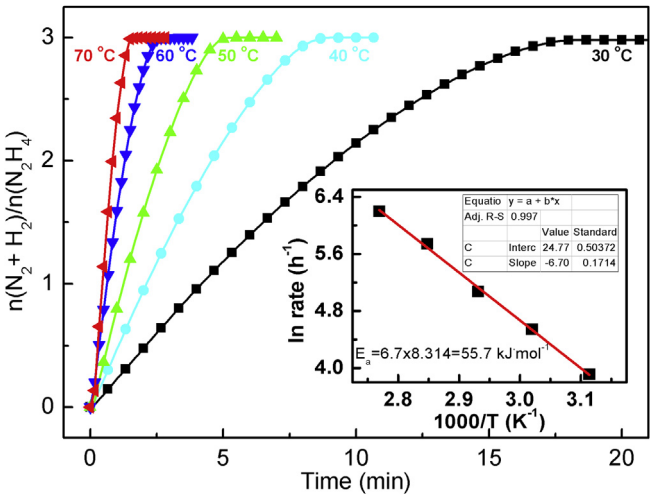

Fig. 6. Decomposition kinetics curves of the system composed of 4 mL of 0.5 M $N_2H_4{\cdot}H_2O$ + 0.5 M NaOH solution and $Ni_{87}Pt_{13}$/MA catalyst at varied temperatures. The catalyst/$N_2H_4{\cdot}H_2O$ molar ratio was fixed at 1:10. The inset gives the Arrhenius treatment of the temperature-dependent rate data for determination of the apparent activation energy.

temperatures. As expected, the reaction rate increases with temperature, *e.g.*, elevating the reaction temperature from 30 to 70 °C caused ~10-fold increase of reaction rate (see in Fig. 6 and Table 2). Interestingly, such kinetics enhancement was achieved without compromise in H_2 selectivity. The decomposition of $N_2H_4{\cdot}H_2O$ over $Ni_{87}Pt_{13}$/MA catalyst exhibits 100% selectivity to H_2 generation at a temperature range of 30–70 °C. This is in sharp contrast to the systems using $Ni_{0.99}Pt_{0.01}$ [13], $Ni_{0.60}Pd_{0.40}$ [17], $Ni_{50}Fe_{50}$ [18], or Ni–Al_2O_3–HT [9] catalysts, which showed considerable temperature-dependence of H_2 selectivity. From a practical point of view, high and temperature-independent selectivity to H_2 generation is clearly a desirable attribute for hydrogen storage application. On the basis of the temperature-dependent rate data, the apparent activation energy of the catalytic decomposition of $N_2H_4{\cdot}H_2O$ over $Ni_{87}Pt_{13}$/MA catalyst was determined to be 55.7 ± 0.2 kJ mol^{-1}, which is comparable to the values for the systems using Ni–Pt [14] or Ni–Al_2O_3–HT [9] catalyst. In addition, the newly developed $Ni_{87}Pt_{13}$/MA catalyst was tested in terms of durability in cyclic usage. As shown in Fig. 7, the $Ni_{87}Pt_{13}$/MA catalyst retained 98% of its initial activity and 100% H_2 selectivity even at its 10th time usage. Such cyclic stability compares favorably with the results of open literature. Presumably, the uniform dispersion of Ni–Pt nanoparticles and strong metal-support interaction arising from the one-pot synthesis process and the confinement of nanoparticles inside the pore channels of MA all contribute to the satisfactory durability of the $Ni_{87}Pt_{13}$/MA catalyst.

Employment of alloying and immobilization strategies had yielded a high-performance Ni–Pt catalyst, which showed superior and stable catalytic activity towards the selective decomposition of $N_2H_4{\cdot}H_2O$ to generate H_2 at mild conditions. But fundamentally, the mechanistic reason for the drastic enhancement of catalytic performance arising upon alloying Ni with Pt remains unclear. To gain insight into this open question, we conducted XPS analysis of the $Ni_{87}Pt_{13}$/MA and relevant monometallic catalysts. As shown in Fig. 8, both Ni and Pt elements showed two chemically different entities that correspond to

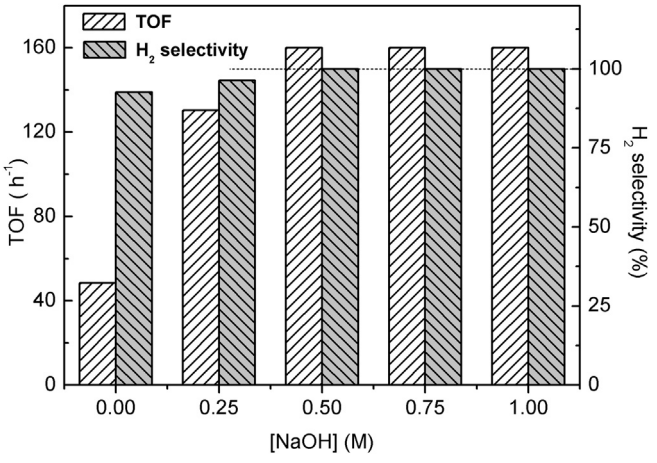

Fig. 5. Effect of NaOH concentration on reaction rate and H_2 selectivity of the system composed of 4 mL of 0.5 M $N_2H_4{\cdot}H_2O$ + x M NaOH solution (x = 0, 0.25, 0.5, 0.75 and 1.0, respectively) and $Ni_{87}Pt_{13}$/MA catalyst at 50 °C. The catalyst/$N_2H_4{\cdot}H_2O$ molar ratio was fixed at 1:10.

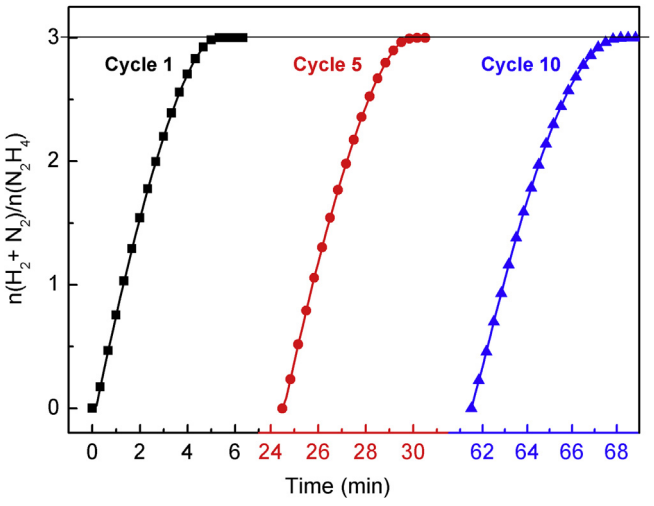

Fig. 7. Cyclic performance of the $Ni_{87}Pt_{13}$/MA catalyst in catalyzing the decomposition of $N_2H_4{\cdot}H_2O$ at 50 °C. The catalyst/$N_2H_4{\cdot}H_2O$ molar ratio was fixed at 1:10.

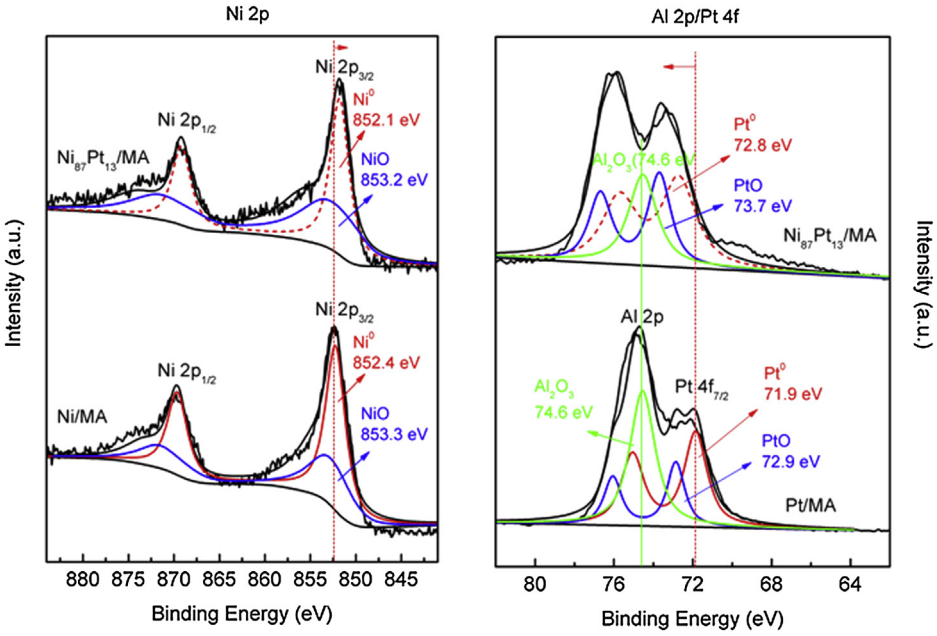

Fig. 8. XPS spectra of Ni/MA, $Ni_{87}Pt_{13}$/MA and Pt/MA catalyst samples. Note: The Pt $4f_{5/2}$ signal interferes with the Al 2p signal.

metallic and oxide states [14,31]. In comparison with the monometallic catalysts, the $Ni_{87}Pt_{13}$/MA catalyst exhibited a negative shift of Ni $2p_{3/2}$ BE of metallic Ni^0 (0.3 eV) and a concurrent positive shift of Pt $4f_{7/2}$ BE of metallic Pt^0 (0.9 eV). These results indicate that Pt acts as an electron donor and its incorporation results in an increase of electron density of Ni active center. As a consequence, back electron donation from Ni to the antibonding orbital of N_2H_4 might be enhanced [32]. This consideration may roughly explain the activity enhancement, but the effect of alloying on H_2 selectivity remains unresolved. In this regard, coupled theoretical and experimental studies are still required for elucidating the relationships between the electronic structure and catalytic performance [33–35], which may provide guideline for the design and synthesis of high-performance heterogeneous catalysts.

4. Conclusions

By using a simple one-pot EISA method, we synthesized a series of Ni–Pt bimetallic catalysts that are composed of tiny alloy nanoparticles immobilized on the mesoporous alumina. These Ni-rich nanocatalysts showed a favorable combination of high catalytic activity, 100% H_2 selectivity and satisfactory durability in promoting hydrogen generation from $N_2H_4 \cdot H_2O$ at mild conditions. For example, the $Ni_{87}Pt_{13}$/MA catalyst enabled a complete decomposition of $N_2H_4 \cdot H_2O$ to generate H_2 within 5 min at 50 °C in the presence of 0.5 M NaOH and retained 98% of its initial activity at its 10th time usage. Such catalytic performance stands out as the top level of the $N_2H_4 \cdot H_2O$ decomposition catalysts reported to date. The facile synthesis of high-performance and cost-effective Ni-based catalyst is of clear significance for the development of $N_2H_4 \cdot H_2O$ as a viable hydrogen carrier.

Acknowledgments

The financial supports for this research from the National Basic Research Program of China (973 program, Grant No. 2010CB631305), the National Outstanding Youth Science Foundation of China (Grant No. 51125003), the National Natural Science Foundation of China (Grant No. 51071155 and 51471168) and Shenyang National Laboratory for Materials Science are gratefully acknowledged.

References

[1] U. Eberle, M. Felderhoff, F. Schüth, Angew. Chem. Int. Ed. 48 (2009) 6608–6630.
[2] C. Weidenthaler, M. Felderhoff, Energy Environ. Sci. 4 (2011) 2495–2502.
[3] P. Wang, X.D. Kang, Dalton Trans. (2008) 5400–5413.
[4] U.B. Demirci, P. Miele, Energy Environ. Sci. 2 (2009) 627–637.
[5] U.B. Demirci, O. Akdim, P. Miele, Int. J. Hydrogen Energy 34 (2009) 2638–2645.
[6] M. Yadav, Q. Xu, Energy Environ. Sci. 5 (2012) 9698–9725.
[7] S.K. Singh, Q. Xu, Catal. Sci. Technol. 3 (2013) 1889–1900.
[8] S.J. Cho, J. Lee, Y.S. Lee, D.P. Kim, Catal. Lett. 109 (2006) 181–186.
[9] L. He, Y.Q. Huang, A.Q. Wang, X.D. Wang, X.W. Chen, J.J. Delgado, T. Zhang, Angew. Chem. Int. Ed. 51 (2012) 6191–6194.
[10] D.G. Tong, W. Chu, P. Wu, G.F. Gu, L. Zhang, J. Mater. Chem. A 1 (2013) 358–366.
[11] S.K. Singh, X.B. Zhang, Q. Xu, J. Am. Chem. Soc. 131 (2009) 9894–9895.
[12] S.K. Singh, Q. Xu, Chem. Commun. 46 (2010) 6545–6547.
[13] S.K. Singh, Z.-H. Lu, Q. Xu, Eur. J. Inorg. Chem. (2011) 2232–2237.
[14] S.K. Singh, Q. Xu, Inorg. Chem. 49 (2010) 6148–6152.
[15] K. Aranishi, A.K. Singh, Q. Xu, ChemCatChem 5 (2013) 2248–2252.
[16] S.K. Singh, Q. Xu, J. Am. Chem. Soc. 131 (2009) 18032–18033.
[17] S.K. Singh, Y. Iizuka, Q. Xu, Int. J. Hydrogen Energy 36 (2011) 11794–11801.
[18] S.K. Singh, A.K. Singh, K. Aranishi, Q. Xu, J. Am. Chem. Soc. 133 (2011) 19638–19641.
[19] L. He, Y. Huang, X.Y. Liu, L. Li, A. Wang, X. Wang, C.-Y. Mou, T. Zhang, Appl. Catal. B 147 (2014) 779–788.
[20] L. He, Y.Q. Huang, A.Q. Wang, Y. Lu, X.Y. Liu, X.W. Chen, J.J. Delgado, X.D. Wang, T. Zhang, J. Catal. 298 (2013) 1–9.
[21] H.L. Wang, J.M. Yan, Z.L. Wang, S.-I. O, Q. Jiang, J. Mater. Chem. A 1 (2013) 14957–14962.
[22] J. Wang, X.-B. Zhang, Z.-L. Wang, L.-M. Wang, Y. Zhang, Energy Environ. Sci. 5 (2012) 6885–6888.
[23] D.G. Tong, D.M. Tang, W. Chu, G.F. Gu, P. Wu, J. Mater. Chem. A 1 (2013) 6425–6432.
[24] S.-I. O, J.M. Yan, H.L. Wang, Z.L. Wang, Q. Jiang, J. Power Sources 262 (2014) 386–390.
[25] J.J. Zhang, Q. Kang, Z.H. Yang, H.B. Dai, D.W. Zhuang, P. Wang, J. Mater. Chem. A 1 (2013) 11623–11628.
[26] A. Chen, T. Miyao, K. Higashiyama, H. Yamashita, M. Watanabe, Angew. Chem. 122 (2010) 10091–10094.
[27] N. Wang, K. Shen, L. Huang, X. Yu, W. Qian, W. Chu, ACS Catal. 3 (2013) 1638–1651.

[28] Q. Yuan, A.X. Yin, C. Luo, L.D. Sun, Y.W. Zhang, W.T. Duan, H.C. Liu, C.H. Yan, J. Am. Chem. Soc. 130 (2008) 3465–3472.
[29] C.J. Brinker, Y.F. Lu, A. Sellinger, H.Y. Fan, Adv. Mater. 11 (1999) 579–585.
[30] S.M. Morris, P.F. Fulvio, M. Jaroniec, J. Am. Chem. Soc. 130 (2008) 15210–15216.
[31] C.D. Wagner, W.M. Riggs, L.E. Davis, J.F. Moulder, G.E. Mulenberg (Eds.), Handbook of X-ray Photoelectron Spectroscopy, first ed., Perkin Elmer Corporation, 1979.
[32] M. Kitano, Y. Inoue, Y. Yamazaki, F. Hayashi, S. Kanbara, S. Matsuishi, T. Yokoyama, S.-W. Kim, M. Hara, H. Hosono, Nat. Chem. 4 (2012) 934–940.
[33] J.K. Nørskov, T. Bligaard, J. Rossmeisl, C.H. Christensen, Nat. Chem. 1 (2009) 37–46.
[34] E. Nikolla, J. Schwank, S. Linic, J. Am. Chem. Soc. 131 (2009) 2747–2754.
[35] H. Xin, A. Holewinski, N. Schweitzer, E. Nikolla, S. Linic, Top. Catal. 55 (2012) 376–390.